Asian Journal of Research and Reviews in Physics

4(3): 1-13, 2021; Article no.AJR2P .68700
ISSN: 2582-5992

Investigation of Proton and Neutron Alignment in the Ba and Ce Isotopes within Interaction Interacting Boson Model and Triaxial Rotor Model

Ali N. Sabbar[1] and Saad N. Abood[1*]

[1]Physics Department, College of Science AL-Nahrain University – Baghdad, Iraq.

Authors' contributions

This work was carried out in collaboration between both authors. Both authors read and approved the final manuscript.

Article Information

DOI: 10.9734/AJR2P/2021/v4i330142
Editor(s):
(1) Dr. Khalil Kassmi, Mohamed Premier University, Morocco.
(2) Dr. Jelena Purenovic, Kragujevac University,Serbia.
(3) Prof. Shi-Hai Dong, National Polytechnic Institute, Mexico.
Reviewers:
(1) Chong Qi, KTH Royal Institute of Technology, Sweden.
(2) Manoj Kumar, Meerut College Meerut. India.
(3) Ratna Dewi Syarifah, University of Jember, Indonesia.
Complete Peer review History: http://www.sdiarticle4.com/review-history/68700

Original Research Article

Received 23 March 2021
Accepted 29 May 2021
Published 05 June 2021

ABSTRACT

In the form of two quasi-particles coupled to a core described by the IBM-1 and Triaxil Rotor models, the high-spin states of the Ba and Ce isotopes are studied. Bands based on both $(vh_{11/2})^{-2}$ and $(\pi h_{11/2})^2$ configurations are considered, which is found to be appropriate for this region to better explain band-crossing systems. Between the recent experimental data and the calculated energy spectra and electric transition probability, fair agreement is achieved.

Keywords: IBM-1; triaxial rotor model; nuclear structure; electric transition probability.

1. INTRODUCTION

In recent years, both experimentally and theoretically, the Xe, Ba and Ce which nuclei are transitional, have been subject to intensive research. In addition to their transitional existence, which makes them suitable for evaluating different collective models, a number of interesting phenomena such as Back-bending and the anomaly of prealignment B(E2) are also seen. Very recently, the Kolin group's experimental efforts resulted in the discovery in

**Corresponding author: E-mail: saadnaji_95@yahoo.com*

$^{128\text{-}130}$Ba of two side bands crossing the ground-state band (gsb) at comparable energies [1,2]. The interpretation of these bands as bands associated with protons and neutrons raises the interesting possibility of a rivalry between configurations of $(\nu h_{11/2})^{-2}$ and $(\pi h_{11/2})^{2}$. A similar situation was observed in the Ce isotopes, where a negative g-factor was calculated for the Back-bending $I0^{+}$ state in ^{134}Ce, suggesting its neutron nature [3], as the Back-bending in ^{130}Ce is known due to blocking arguments with the $h_{11/2}$ proton alignment [4]. Since only one form of configuration was used in previous theoretical studies of high-spin states [5-7], a new study of the experimental results, which takes both proton and neutron degrees of freedom into account simultaneously, is needed.

By specifically connecting two quasi-particles to the core states, the orthodox interpretation of Back-bending in terms of the crossing of the ground state band by a two-quasi-particle band has been integrated into a variety of phenomenological collective models. Of these, the triaxial rotor [8,9] and IBM models [5,6,10,11] that will be used in the present work are listed in particular. In separate nuclear regions, both models have been effective in explaining back-bending. We will first include a brief overview of the triaxial rotor and the two-quasi-particle models of the IBM plus. Applications will concentrate on ^{128,130}Ba and ^{134}Ce, where the recent occurrence of double crossing has been observed. The experimental data will be compared with detailed calculations of the energy spectrum and electromagnetic properties.

Furthermore, the negative-energy spectra measured with the same model will be provided in the rotor case. The IBM model will discuss the band-crossing systematics and the transition between the configurations of the proton and neutron.

2. THEORETICAL CONSIDERATIONS

2.1 IBM-1 plus Two-Quasi-Particle Model

Since in the literature [10,12] the model (to be called IBM+2q.p.) is discussed, here we simply state the Hamiltonian used in the calculations:

$$H = H_B + H_F + H_{BF} + H_{mix} \quad (1)$$

Since it is empirically understood that the quadrupole force acts between nucleons with different charges, quasi-particles of the neutron can only interact with the protons in the core and

For the Hamiltonian of IBM [13] H_B we use the simplified version:

$$H_B = \varepsilon n_d + \kappa' L.L + \kappa Q.Q \quad (2)$$

where the boson quadrupole operator contains a further parameter χ:

$$Q = (s^{+}d^{\sim} + d^{+}s^{\sim})^{(2)} + \chi(d^{+}d^{\sim})^{(2)} \quad (3)$$

The Hamiltonian of effective fermion H_F restricted to a single *j*-shell takes the form:

$$H_F = \sum_m \varepsilon_j a^{+}_{jm} \times a^{\sim}_{jm} + \frac{1}{2}\sum_{JM} V^{J}\left[a^{+}_{j}a^{+}_{j}\right]^{JM}\left[a_j a_j\right]^{JM} \quad (4)$$

Here, for the residual interaction V^{j}. The last two terms characterize the interaction of the boson-fermion H_{BF} conserves, respectively, fermion and boson numbers,

$$H_{BF} = \Gamma_0(u_j^2 - \upsilon_j^2)q_{jj}\left(\left[s^{+}d^{\sim} + d^{+}s^{\sim}\right]^2 + \chi\left[d^{+}d^{\sim}\right]^2\right)\left[a^{+}a^{\sim}\right]^2 - \Gamma_0 20 u_j \upsilon_j q_{jj}\sqrt{\frac{2N}{2j+1}}\left[\left[d^{+}a^{\sim}_{j}\right]^{j}\left[d^{\sim}a^{+}_{j}\right]^{j}\right]^{0} \quad (5)$$

Whereas H_{mix} preserves only the complete number of nucleons, combining zero and two bands of quasi-particles,

$$H_{mix} = \Gamma_0 5\sqrt{\frac{1}{2}}(u_j^2 - \upsilon_j^2)q_{jj}\frac{1}{\sqrt{2j+1}}\left\{s^{+}\left[a_j a_j\right]^{0} + h.c.\right\} + \left[\Gamma_0 u_j \upsilon_j q_{jj}\sqrt{N} + V^2\sqrt{\frac{1}{2}}(u_j^4 + \upsilon_j^4)\right]\left\{d^{+}\left[a_j a_j\right]^{2} + h.c.\right\} \quad (6)$$

The coupling strengths in Eqns.(5) and (6l) are Γ_0, χ, u_j and υ_j are the BCS. Occupation amplitudes, q_{jj} denotes the matrix element of the decreased quadrupole and *N* is the number of the boson. We emphasize that, by invoking a number-conserving quasi-particle transformation, Eqns.(5) and (6) are derived from the regular boson-fermion quadrupole strength.

vice versa. The proton and neutron bosons are not distinct in the formalism of the IBM-1, used here for simplicity. Since it is empirically understood that the quadrupole force acts between nucleons with different charges, only the protons in the core and vice versa can interact with quasi-particles of the neutron. In the formalism of the IBM-1, used here for simplicity, the proton and neutron bosons are not distinct.

$$\Gamma_0 = \frac{N_\pi(v)}{N}\kappa_0 \quad (7)$$

Where κ_0 is a quadruple strength overall. The Hamiltonian, Eq.(1), is diagonalized in the basis

$$\left| m\beta J_1, n\gamma J_2; J \right\rangle \quad (8)$$

Here, the boson (fermion) system's complete spin is denoted by J_1, (J_2) and the number of valence nucleons is set by 2m+n. In ^{130}Ba, for example, $N = N_\pi + N_\nu$ = 3 +4 = 7 and the basis consists of three parts: (i) m = N, the ^{130}Ba core is represented by n = 0; (ii) $m = n-1$, $n = 2$ (protons) - two-proton $q.p$. The ^{128}Xe core excitations; and (iii) $m = N-1$, $n = 2$ (neutrons) - two-neutron $q.p$. The ^{132}Bacore was based on excitations.

The IBM-1 Hamiltonian parameters, along with a comparison of the experimental data, are shown in Table (1). Note that there are 6 to 9 bosons in each isotope chain. The quadrupole strength κ is increased linearly with the number of protons, driven by a microscopic picture [14]. A gradual increase in χ is simulated by the onset of deformation ($(O(6) \to SU(3)$ transformation in the IBM-1 picture). Finally, the single-boson energy E is adapted to the first state of 2^+, which has a value of approximately 0.500 MeV. The above-mentioned choice of parameters does not include the effect of two-quasi-particle states in which low-lying levels are pressed down. ε is raised by about 10% in the actual calculations to cancel this effect.

2.2 Triaxial Rotor Model

The model (referred to as Rot+ $2q.p$) has been discussed and analyzed in the literature previously [8,9]. As a result, we only provide an overview of the model here in order to keep the topic manageable, and we direct the reader to the above references for more details. The Hamiltonian is written as:

$$H = \sum_{i=1}^{3}\frac{R_n^2}{2\theta_n} + \sum_\alpha \varepsilon_a c_a^+ c_a + \frac{1}{2}\sum_{abcd}\langle ab|\upsilon_{res}|cd\rangle N(c_a^+ c_b^+ c_c c_d)$$
$$-k\sum_{ab}\left\langle a\left|\cos\gamma Y_{20} + \sqrt{\frac{1}{2}}\sin\gamma(Y_{22}+Y_{2-2})\right|b\right\rangle c_a^+ c_b \quad (9)$$

The first term defines a triaxial rotor, while the second term explains two quasi-particles that are connected by the third term. We use the surface-delta interaction (SDI) [4] for the residual interaction. This Hamiltonian is diagonalized in the quasi-weak basis, which is more suitable for core state truncation than the strict coupling basis:

$$\left| IM;\alpha R = 1\right\rangle = \left|\alpha I\right\rangle \left| BCS\right\rangle$$
$$\left| IM;(j_1 j_2)j,\alpha R\right\rangle = \left[(\beta_{j1}^+ \beta_{j2}^+)j\left|\alpha R\right\rangle\right]_{IM}\left| BCS\right\rangle \quad (10)$$

The spherical quasi-particle operator is denoted by β. Since particles in high-j orbits are easiest to coordinate, the single-particle basis for positive-parity states is limited to the proton and neutron $h_{11/2}$. In the case of negative-parity states, the basis includes all neutron levels in the 50-82 closed shell, as well as protons levels ($h_{11/2}$, $g_{7/2}$, and $d_{5/2}$, The core states are truncated as follows in order to keep the problem's dimension manageable:

$$R \le 10 - 2\alpha \quad \text{for } 12 \le I \le 18$$
$$R \le 8 - 2\alpha \quad \text{for } I = 0,\ 10,\ 18$$
$$R \le 6 - 2\alpha \quad \text{for } 2 \le I \le 9 \quad (12)$$

The ground and gamma bands are represented by $\alpha = 0,1$ respectively.

The energies and B(E2) values of the first and second 2^+ levels are equipped with the β- and γ -deformation parameters, which agree with Meyer-ter-Vehn's values used in his measurement of neighboring odd nuclei [15]. The BCS equations with a pairing strength $G = 37/A$ yield the values for the gap Δ and the Fermi level λ. The Fermi levels are rotated up and down in order to find a better match for the quasi-particle bands. However, minor variations in

Fermi levels are found to have little effect on the effects. As a result, the BCS values in Table 1 have been adjusted, with the exception of λ_π, in ^{130}Ba, which has been moved up 0.200 MeV, to achieve better agreement for the positive-parity high-spin states.

From a fit to the ^{130}Ba states, the residual intensity interaction is set at *K* = 0.33 MeV. To reduce the strength of the higher multipole terms and simulate the increased collectivity of the lower spin states, angular momentum dependence is introduced in K for the negative-parity states, as in the previous work [9]:

$$K_j = K[1 + 0.02j(j+1)]^{-1} + \Delta K_j \qquad (13)$$

3. RESULTS AND DISCUSSION

In the IBM-1, detailed positive-parity spectrum calculations for $^{128\text{-}130}$Ba and ^{134}Ce are compared to the experimental level schemes in the Figures (2-4). Overall, in the Ba isotopes, there is a clear agreement between the experimental and calculated spectra. Only g-factor measurements will overcome minor inconsistencies between the two versions, such as the existence of the first crossing band. In ^{134}Ce, owing to a sudden change in the properties of this nucleus, the situation is more complicated. As shown in Table (1) compared with its neighbors, ^{134}Ce is much less deformed. In addition, the negative g-factors [4] $g(10_1^+)) = -0.19(1)$, $g(10_2^+)) = -0.30(25))$ suggesting their neutron nature were calculated for both crossing $l0^+$ states. Nevertheless, reviewing Fig.(4) shows that the $q.p$ -proton .The band matches the second crossing band experimental levels much better than the second neutron $q.p$ in the model. We also expanded the calculations to the $^{126\text{-}\ 130}$Ba and $^{130\text{-}134}$Ce isotopes in the IBM+2q.p model in order to add more light to this matter and to better understand the band-crossing mechanism.

The results for the proton and neutron $q.p$ -bands are shown in Fig. alongside the experimental assignments. It follows from the semi-microscopic picture (Eqns. (5)-(6)) that with increasing boson number, the interaction strength for protons increases (decreasing mass number because neutrons are holes) and decreases for neutrons. In addition to the deformation effect (i.e. Table (2)), the model predicts that with the decreasing mass number, the proton $q.p$-band decreases and its inertial moment increases slightly, while the neutron $q.p$-band increases with a strong increase in its inertial moment. These trends are clearly observed in our estimates and the existing ones. If we define the states of the experiment as in Fig.(4), experimental data. Therefore, the energy systematics clearly suggests the existence of a proton $q.p$. The band in the band-crossing region at ^{134}Ce also predicts a neutron $q.p$-band above the proton band at ^{l26}Ba and $^{130\text{-}132}$Ce if not already observed.

In order to illustrate the band structures in the two models, we give in Table 3 the main components of the high-spin states. The main observations are: (i) the IBM+2q.p. wave functions are relatively purer compared to the Rot+ 2q.p. wave functions (which is true also for the low-lying levels); (ii) the aligned bands are dominated by the configuration $[R \times (h_{11/2})^2_{j=10}]_{J=R+10}$ where *R* is the core angular momentum; and, (iii) the proton $q.p$ -band is less aligned than the neutron $q.p$ -band. A direct test of these predictions requires a detailed knowledge of the electromagnetic properties which is lacking at present. However, for (i) one can indirectly infer from the energy spectra (Figs. 2-4) that the truth is somewhere in between, since the experimental 10_1^+ and 12_1^+ levels lie in between the predictions of the two models. (The more mixing there is, the more the ground-band states are pressed down.).

In the single-particle Hamiltonian, the usual Nilsson parameters are used:
$\hbar\omega = 41/A^{1/3}$ MeV, $\kappa_{\pi,\nu} = 0.0640$, $\mu_\pi = 0.62$, $\mu_\nu = 0.44$ .The empirical relation [16] is used to evaluate the coupling constant:

$$k = \left(\frac{16}{5}\pi\right)^{1/2} 206A^{-1/3} \quad MeV \qquad (14)$$

Table (1) lists some of the remaining parameters.

The occupation probabilities υ_j^2 are obtained by spherically averaging the Nilsson+BCS shell

Table 1. IBM-1 Hamiltonian parameters for Xe, Ba, Ce isotopes (in MeV) except χ is dimensionless

parameter	Xe				Ba				Ce			
	^{122}Xe	^{124}Xe	^{126}Xe	^{128}Xe	^{126}Ba	^{128}Ba	^{130}Ba	^{132}Ba	^{130}Ce	^{132}Ce	^{134}Ce	^{136}Ce
ε	0.545	0.515	0.500	0.510	0.480	0.465	0.480	0.550	0.465	0.490	0.550	0.660
κ	-0.22	-0.22	-0.22	-0.22	-0.25	-0.25	-0.25	-0.25	-0.28	-0.28	-0.28	-0.28
κ'	-0.06	-0.06	-0.06	-0.06	0.07	0.07	0.07	0.07	0.07	0.07	0.07	0.07
χ	-0.45	-0.35	-0.25	-0.15	-0.50	-0.50	-0.35	-0.20	-0.45	-0.30	-0.15	0.0

Table 2. Deformation and BCS parameters used in the Rot +2q.p. model

Isotope	β	γ	Δ_π (MeV)	λ_π (MeV)	Δ_ν (MeV)	λ_ν (MeV)
^{128}Ba	0.23	24^0	1.048	45.223	1.298	48.5
^{130}Ba	0.23	26^0	1.005	45.001	1.133	49.33
^{134}Ce	0.20	24^0	1.246	44.421	1.100	49.4

Table 3. Occupation probabilities and quasi-particle energies for the $h_{11/2}$ protons and neutron holes in Ba and Ce isotopes

Isotopes	υ_ν^2	υ_π^2	ε_ν (MeV)	ε_π (MeV)
^{126}Ba	0.521	0.11	1.681	2.151
^{128}Ba	0.441	-	-	-
^{130}Ba	0.370	-	-	-
^{130}Ce	0.431	0.151	-	1.852
^{132}Ce	0.349	-	-	-
^{134}Ce	0.258	-	-	1.977

occupancies used in the Rot+2q.p. for the $h_{11/2}$ single-particle levels considered here. The calculations are given in Table 2. The average BCS results are too crude for the quasi-particle energies and therefore have to be resealed. Since the $vh_{11/2}$ shell is filled by neutrons in this region, ε_ν changes very little and is considered to be constant. The decrease in ε_π, from Ba to Ce isotopes, reflects the fact that the level of Fermi is closer to the shell of $\pi h_{11/2}$. The case of ^{134}Ce is an exception and discussed.

The SD1 is set to 0.3 MeV, which corresponds to the BCS pairing strength $G = 37/A$. $\kappa_\nu = 0.200$ MeV, $\kappa_\pi = 0.125$, $\chi_{\pi,\nu} = -0.200$ are the boson-fermion coupling strengths fitted in ^{130}Ba and kept constant for the other nuclei. The results are found to be unaffected by changes in χ. In the E2 transformation operator, a positive value of $\chi_{\pi,\nu}$, $\chi_{\pi,\nu} = -0.200$ is used, which appears to be needed to reproduce the branching ratios. Since the mass and charge distributions in the nucleus will vary, the quadrupole operators used in the Hamiltonian and transition operators are different. Furthermore, χ is only a perturbative component of the quadrupole operator in this case? The other parameters required for calculating electromagnetic properties are the same as those mentioned in the previous section.

Only the three largest components with minimum squared amplitude of 0.10 are shown. In parentheses, the basis states are mentioned. Members of the group g and γ are denoted by the subscripts g and γ. π and ν refer to the proton and neutron nature of the two quasi-particles, respectively. The first entry for each state comes from Rot+ 2q.p. The first is from the IBM+2q.p model, and the second is from the Rot+ 2q.p model.

3.1 Electric Transition Probability

The effective charges $e_\pi = 11.38 \quad W.u$ and $e_\nu = 1.33 \quad W.u$ were used to evaluate the electromagnetic properties which has been normalized to experimental $B(E2;2_1^+ \to 0_1^+)$. In Table (4), we show the B(E2) transition rates for ^{130}Ba and ^{134}Ce. Although the results of the IBM+2q.p. model traces the experimental data better due to the boson cut-off, both models are far from explaining the drop in the B(E2) values which is a general feature of all nuclei in this region and has been called the “pre-alignment B(E2) anomaly” [7]. Noting that even a more fundamental theory like MONSTER has been unable to explain this drop [17], and in the face of experimental uncertainties, we postpone further

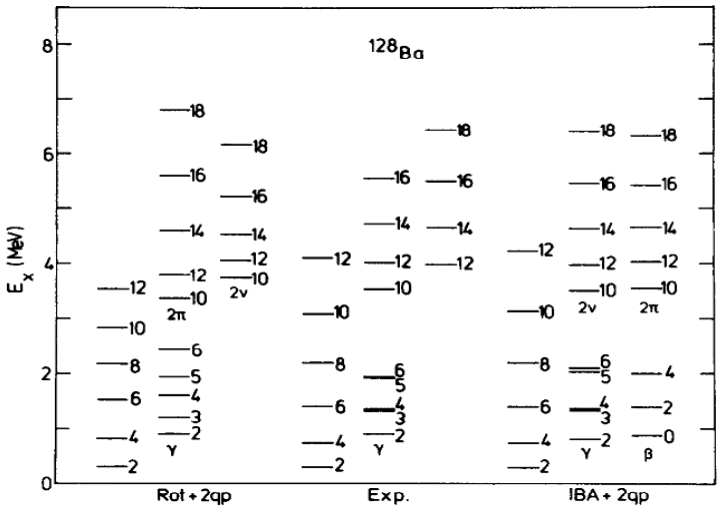

Fig. 1. Energy spectra in ^{128}Ba, calculated and experimental data [18]; The proton and neutron, 2-quasi-particle bands are shown by 2π and 2ν

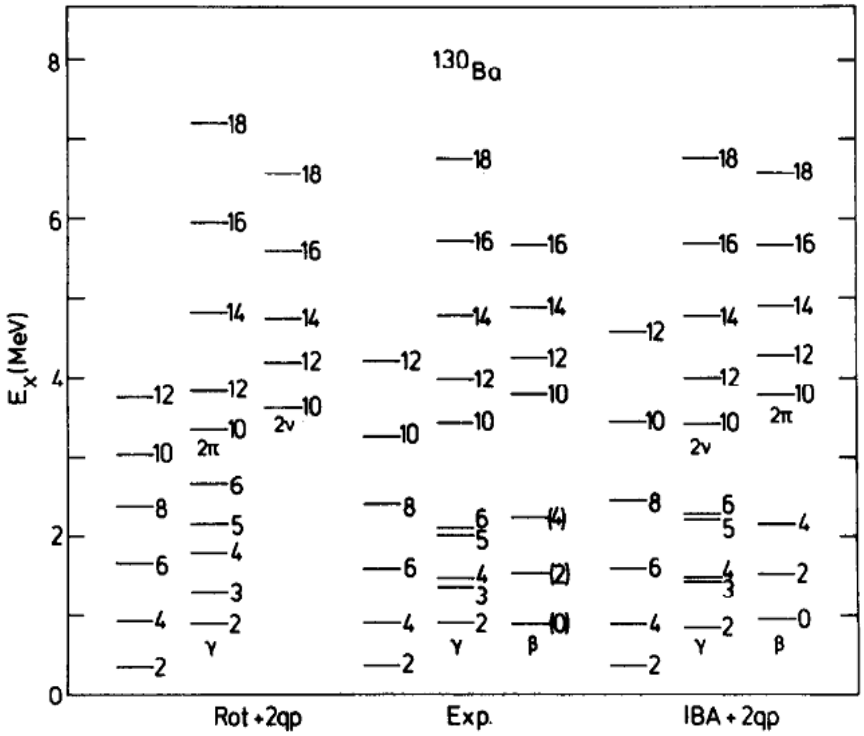

Fig. 2. Calculated and Experimental data [19] for ^{130}Ba isotope

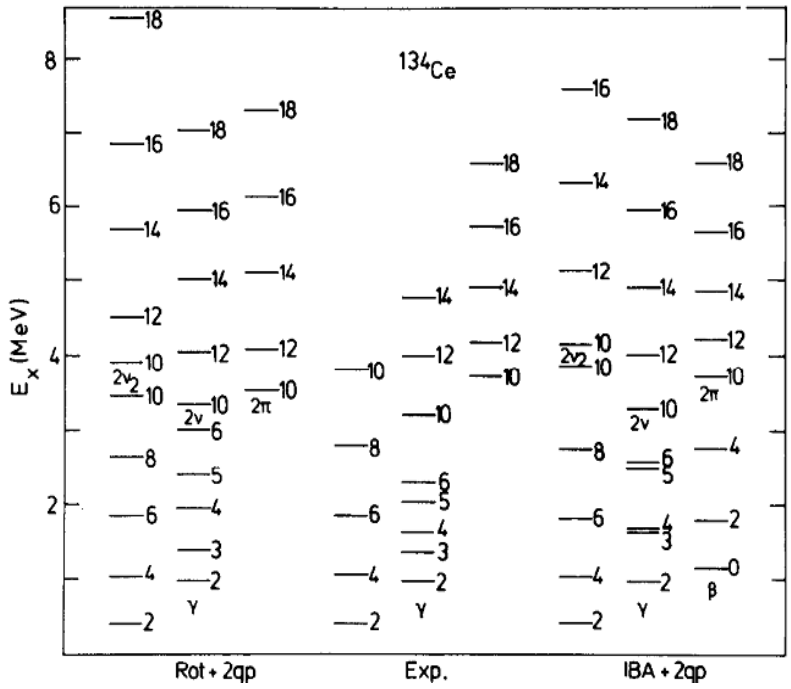

Fig. 3. Calculated and Experimental data [20] for ^{134}Ce isotope, where $2\nu_2$ indicates the two-neutron q.p. band

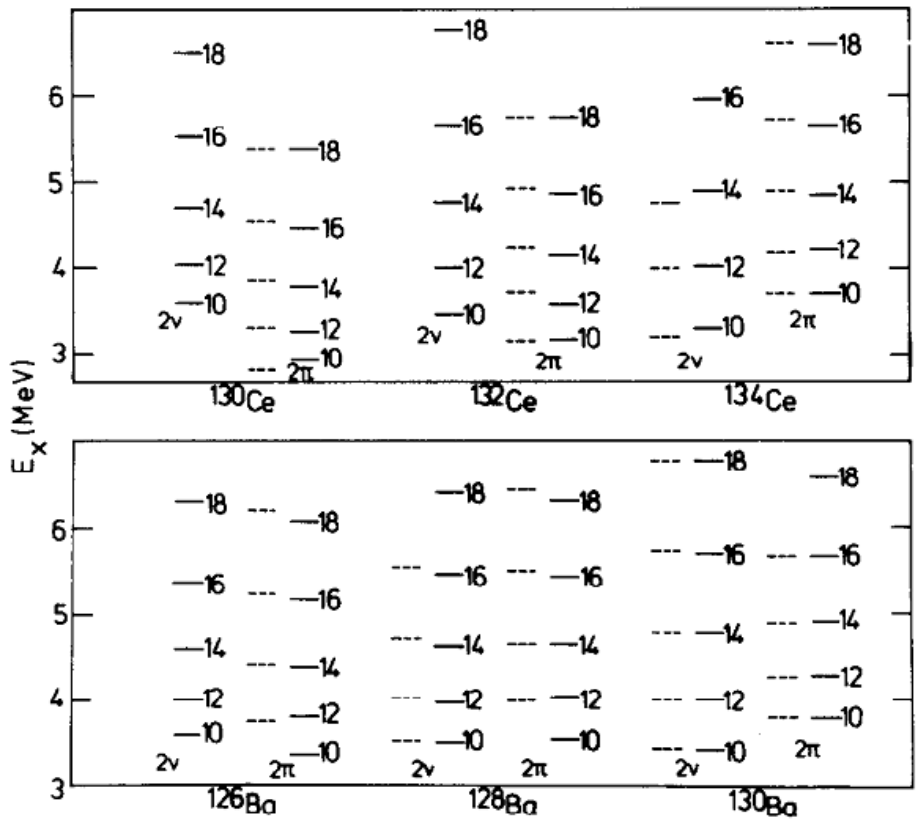

Fig. 4. The IBA+2q.p. model was used to calculate high-spin systematics in $^{126\text{-}130}$Ba and $^{130\text{-}134}$Ce. The experimental data (dashed lines) are from the references [18,19, 20,21,22, 23]

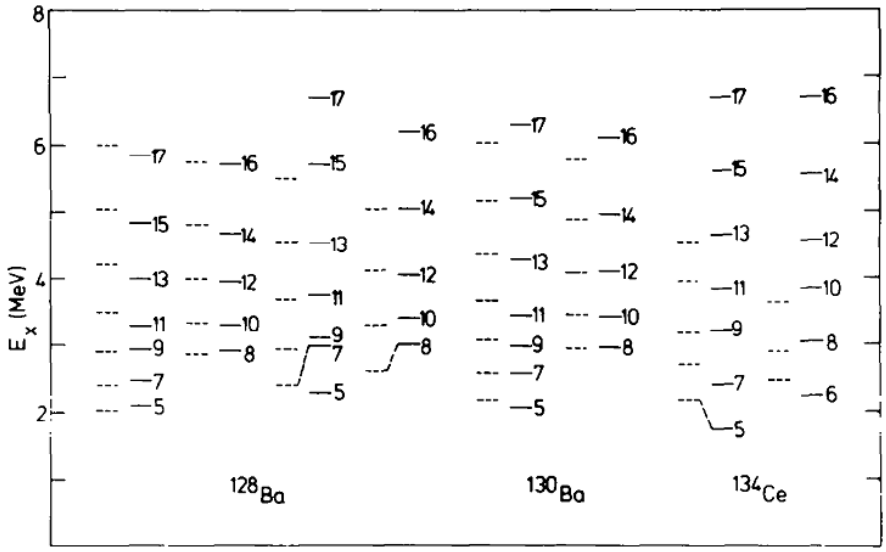

Fig. 5. The Rot+2q.p. mode was used to calculate the negative-parity energy spectra in $^{128\text{-}130}$Ba and ^{134}Ce. The experimental (dashed lines) data are taken from refs. [18,19,20]

Table 4. positive parity high spin states in ^{130}Ba and ^{134}Ce isotopes

^{130}Ba			
g- band			
10	$0.57(10_g)$	$0.11(8_g \times 2_\nu)$	
	$0.90(10_g)$		
12	$0.43(12_g)$	$0.10(10_g \times 2_\nu)$	
	$0.90(12_g)$		
2ν **band**			
10	$0.56(0_g \times 10_\nu)$	$0.30(2_g \times 10_\nu)$	
	$0.92(0_g \times 10_\nu)$	-	
12	$0.52(2_g \times 10_\nu)$	$0.10(4_g \times 10_\nu)$	$0.13(2_\gamma \times 10_\nu)$
	$0.96(2_g \times 10_\nu)$		
14	$0.64(4_g \times 10_\nu)$	$0.17(6_g \times 10_\nu)$	
	$0.98(4_g \times 10_\nu)$	-	
16	$0.77(6_g \times 10_\nu)$	$0.14(8_g \times 8_\nu)$	
18	$0.83(8_g \times 10_\nu)$	$0.12(10_g \times 8_\nu)$	
	$0.98(8_g \times 10_\nu)$	-	
2π band			
10	$0.31(0_g \times 10_\pi)$	$0.31(2_g \times 10_\pi)$	$0.12(4_g \times 10_\pi)$
	$0.42(0_g \times 10_\pi)$	$0.37(2_g \times 10_\pi)$	
12	$0.36(2_g \times 10_\pi)$	$0.18(4_g \times 10_\pi)$	$0.11(2_\gamma \times 10_\pi)$
	$0.58(2_g \times 10_\pi)$	$0.16(4_g \times 10_\pi)$	$0.14(2_\gamma \times 10_\pi)$
	$0.34(4_g \times 10_\pi)$	$0.16(6_g \times 10_\pi)$	$0.20(4_\gamma \times 10_\pi)$

14	$0.69(4_g\times10_\pi)$	$0.10(6_g\times10_\pi)$	$0.13(4_\gamma\times10_\pi)$
16	$0.51(6_g\times10_\pi)$	$0.16(8_g\times10_\pi)$	$0.17(8_\gamma\times8_\pi)$
	$0.83(6_g\times10_\pi)$	$0.10(6_g\times10_\pi)$	
18	$0.71(8_g\times10_\pi)$	$0.16(10_g\times8_\pi)$	
	$0.90(8_g\times10_\pi)$	$0.16(68_g\times8_\pi)$	
^{134}Ce g-band			
10	$0.52(10_g)$	$0.14(8_g\times2_\nu)$	
	$0.88(10_g)$		
12	$0.32(12_g)$	$0.13(3_\gamma\times10_\nu)$	$0.13(4_g\times8_\nu)$
	$0.88(12_g)$		
2ν -band			
10	$0.46(0_g\times10_\nu)$	$0.40(2_g\times10_\nu)$	
	$0.83(0_g\times10_\nu)$	$0.14(2_g\times10_\nu)$	
12	$0.23(2_g\times10_\nu)$	$0.30(2_g\times10_\pi)$	$0.12(2_\gamma\times10_\nu)$
	$0.87(2_g\times10_\nu)$		
14	$0.65(4_g\times10_\nu)$	$0.12(6_g\times8_\nu)$	
	$0.90(4_g\times10_\nu)$		
16	$0.49(6_g\times10_\nu)$	$0.10(10_g\times8_\nu)$	
	$0.90(4_g\times10_\nu)$		
18	$0.78(8_g\times10_\nu)$	$0.10(10_g\times8_\nu)$	
	$0.98(8_g\times10_\nu)$		
2π -band			

10	0.39($0_g \times 10_\pi$)	0.33($2_g \times 10_\pi$)	
	0.56($0_g \times 10_\pi$)	0.31($2_g \times 10_\pi$)	
12	0.24($2_g \times 10_\pi$)	0.17($2_g \times 10_\nu$)	0.15($2_\gamma \times 10_\nu$)
	0.72($2_g \times 10_\pi$)	0.10($4_g \times 10_\pi$)	
14	0.52($4_g \times 10_\pi$)	0.13($6_g \times 10_\pi$)	0.11($6_g \times 8_\pi$)
	0.83($4_g \times 10_\pi$)		
16	0.64($6_g \times 10_\pi$)	0.10($8_g \times 10_\pi$)	0.14($8_g \times 8_\pi$)
	0.90($6_g \times 10_\pi$)		
18	0.75($8_g \times 10_\pi$)	0.11($10_g \times 80_\pi$)	
	0.90($8_g \times 10_\pi$)		
$2\nu_2$ band			
10	0.45($2_g \times 8_\nu$)	0.22($4_g \times 6_\nu$)	
	0.81($2_g \times 8_\nu$)	0.10($4_g \times 6_\nu$)	
12	0.18(12_g)	0.19($3_\gamma \times 10_\nu$)	0.14($2_g \times 10_\nu$)
	0.62($4_g \times 8_\nu$)	0.16($2_\gamma \times 10_\nu$)	
14	0.22($6_g \times 10_\nu$)	0.31($6_g \times 8_\nu$)	0.17($5_g \times 10_\nu$)
	0.85($6_g \times 8_\nu$)	0.10($4_\gamma \times 10_\nu$)	
16	0.28($8_g \times 10_\nu$)	0.40($8_g \times 8_\nu$)	0.12($7_\gamma \times 10_\nu$)
	0.70($8_g \times 8_\nu$)	0.23($6_\gamma \times 10_\nu$)	
18	0.32($10_g \times 10_\nu$)	0.59($10_g \times 8_\nu$)	0.12($7_\gamma \times 10_\nu$)
	0.70($8_g \times 8_\nu$)	0.23($6_\gamma \times 10_\nu$)	

Table 5. Electric Transition Probability $B(E2;J_i^+ \to J_f^+)$ in $W.u$ units

Transitions	^{130}Ba			^{134}Ce		
	Exp. [18]	**IBM+2qp**	**Rot+2qp**	**Exp.** [20]	**IBM+2qp**	**Rot+2qp**
$2_1^+ \to 0_1^+$	57.9 (17)	55.65	60.33	52 (5)	52	55.98
$4_1^+ \to 2_1^+$	78.9 (13)	79.02	81.4	39(8)	46.69	48.21
$6_1^+ \to 4_1^+$	94 (6)	87.2	90.27	-	92.11	90.11
$2_2^+ \to 2_1^+$	-	55.23	57.21	-	45.5	49.08
$3_1^+ \to 2_1^+$	-	100.3	99.24	-	98.33	89.2

discussion of the B(E2) values until ew experiments, planned for the near future, clarify the situation. The most direct way of determining the nature of a $q.p$ -band is by measuring g-factors of the crossing states which have relatively longer lifetimes. In Table 4, we present the g-factor results for the 10^+ and 12^+ members of various bands. As mentioned above, g-factor measurements are available only in ^{134}Ce [ref.[4] and it is difficult to reconcile those results with the calculated energy spectrum (Fig. 4). A radical solution of the problem, suggested in ref. [24], is that the first $l0^+$ state may be an yrast trap as suggested by its much longer lifetime and therefore be outside of the model space. In this case the second band may be the neutron $q.p$ -band and the proton $q.p$ -band remains to be observed. In ^{134}Ce, the higher spin states have a similar structure as the Ba isotopes. At lower spins, however, neutron pairs are more involved and in some cases even they are the dominant components.

4. CONCLUDING REMARKS

The recent experimental data on $^{128\text{-}130}$Ba and ^{134}Ce have been analyzed with the IBM+2q.p. models. Both models are successful in reproducing the main features of the energy spectra, though some discrepancies remain, especially in ^{134}Ce where it is hard to reconcile the g-factor measurements with the calculated spectra. Study of energy systematics in the Ce isotopes suggests the existence of a neutron aligned band in $^{130\text{-}132}$Ce, and a proton aligned band in ^{134}Ce near the band-crossing region. More experimental work is needed to clarify the band structures in these nuclei. The model is unable to explain the prealignment B(E2) anomaly and they should be extended if the phenomenon is proven to be a genuine effect. Both models are unable to describe the pre-alignment B(E2) anomaly, and if the phenomenon is shown to be a true effect, they should be expanded.

COMPETING INTERESTS

Authors have declared that no competing interests exist.

REFERENCES

1. Schiffer K, Dewald A, Gelberg A, Reinhardt R, Zell KO, von Brentano P, Sun Xiangfu, Z. Phys. 1983;A313:245.
2. Sun Xiangfu W, Gast A, Gelberg U, Kaup A, Dewald KO, Zell, P. von Brentano, Phys. Rev. 1983;C28:1167.
3. Zemel A, Broude C, Dafni E, Gelberg A, Goldberg MB, Gerber J, Kumbarttki GJ, Speidel KH. Nucl. Phys. 1982;A383:165.
4. Nolan PJ, Todd DM, Smith PJ, Love DJG, Twin PJ, Andersen0, Garrett JD, Hagemann GB, B. Herskind, Phys. Lett. 1982;108B:269.
5. Gelberg A, Zemel A. Phys. Rev. 1980;C22:937.
6. Yoshida N, Arima A, Otsuka T. Phys. Lett. 1982;114B:86.
7. Draayer JP, Han CS, Weeks KJ, Hecht KT. Nucl. Phys. 1981;A365:127.
8. Yadav HL, Toki H, Faessler A. Phys. Rev. Lett. 1977;39:1128; Phys. Lett. 1978;76B:144; Z. Phys. 1978;AZS7:121.
9. Petrovici A, Faessler A. Nucl. Phys. 1983;A395:44.
10. Morrison I, Faessler A, Lima C. Nucl. Phys. 1981;A372:13.
11. Kuyucak S, Faessler A, Wakai M. Nucl. Phys. 1984;A420:83.
12. Faeqsler A. Rep. Prog. Phys. 1982;45: 653.

13. Arima A, Iachello F. Ann. Rev. Nucl. Part. Sci. 1981;31:75.
14. Talmi I. Int. School of Physics “Enrico Fermi. 1983;87:3.
15. Meyer-ter-Vehn J. Nucl. Phys. 1975;A249:I1 1, 141.
16. Meyer-ter-Vehn J, Stephens FS, Diamond RM. Phys. Rev. Lett. 1974;32:1383.
17. Hammaren E, Schmid KW, Griimmer F, Faessler A. to be published;2021.
18. Kanbe M, Kito K. Nuclear Data Sheets. 200193(33):143.
19. Balraj Singh. Nuclear Data Sheets. 2001;94(227):335.
20. A. Sonzogni. Nuclear Data Sheets. 2004;103:112.
21. Balraj Singh. Nuclear Data Sheets. 2001;94(227):184.
22. Khazov Yu, Rodionov AA, Sakharov S, Balraj Singh. Nuclear Data Sheets 2005;104:687.
23. Katakura J, Kitao K. Nuclear Data Sheets. 2002;97(765):876.
24. Miiller-Veggian M, Beuscher H, Haenni DR, Lieder RM, Neskakis A, Nucl. Phys. 1984;A417:189.

Peer-review history:
The peer review history for this paper can be accessed here:
http://www.sdiarticle4.com/review-history/68700